

PROCEEDINGS OF SPIE

[SPIDigitalLibrary.org/conference-proceedings-of-spie](https://spiedigitallibrary.org/conference-proceedings-of-spie)

Comprehensive modeling of coupled spin-charge transport and magnetization dynamics in STT-MRAM cells

Fiorentini, Simone, Ender, Johannes, Mohamedou, Mohamed, Selberherr, Siegfried, L. de Orio, Roberto, et al.

Simone Fiorentini, Johannes Ender, Mohamed Mohamedou, Siegfried Selberherr, Roberto L. de Orio, Wolfgang Goes, Viktor Sverdlov, "Comprehensive modeling of coupled spin-charge transport and magnetization dynamics in STT-MRAM cells," Proc. SPIE 11470, Spintronics XIII, 114701B (20 August 2020); doi: 10.1117/12.2567480

SPIE.

Event: SPIE Nanoscience + Engineering, 2020, Online Only

Comprehensive modeling of coupled spin-charge transport and magnetization dynamics in STT-MRAM cells

Simone Fiorentini¹, Johannes Ender¹, Mohamed Mohamedou¹, Siegfried Selberherr²,
Roberto L. de Orio², Wolfgang Goes³, and Viktor Sverdlov^{1,2}

¹Christian Doppler Laboratory for Nonvolatile Magnetoresistive Memory and Logic at the

²Institute for Microelectronics, TU Wien, Gusshausstraße 27–29/E360, 1040 Vienna, Austria

³Silavco Europe Ltd., Cambridge, United Kingdom

ABSTRACT

We employ a finite element discretization scheme to solve numerically the coupled spin and charge transport equations in spin-transfer torque magnetoresistive random access memory cells. To adapt the drift-diffusion formalism to the case of a magnetic tunnel junction, we model the tunnel barrier as a material with a low magnetization-dependent conductivity and a large spin diffusion constant. This generalized spin and charge drift-diffusion approach is applied to determine the torques entering the Landau-Lifshitz-Gilbert equation to describe the magnetization dynamics. In particular, the switching times under a fixed voltage, a fixed current, and a fixed current density are compared.

Keywords: Spin and charge drift-diffusion, spin-transfer torque, magnetic tunnel junctions, STT-MRAM

1. INTRODUCTION

Spin-transfer torque magnetoresistive random access memory (STT-MRAM) is an emerging non-volatile memory which is compatible with CMOS technology and is rapidly conquering the market.^{1–7} STT-MRAM possesses an endurance much higher than that of flash memory. STT-MRAMs' access times can be tuned in a broad range. This positions STT-MRAM as a universal memory capable to replace both, static random access memory and flash memory.

The spin-transfer torque is created by a non-equilibrium spin accumulation acting on the magnetization via the exchange interaction. A simultaneous solution of the spin-charge transport equations coupled to the Landau-Lifshitz-Gilbert equation is required to describe the magnetization dynamics for STT-MRAM modeling. In a spin valve, where the ferromagnetic layers are separated by a metal, the spin-charge transport is described by the carriers' drift and diffusion. However, STT-MRAM contains a magnetic tunnel junction (MTJ), and the applicability of this approach is questionable. We demonstrate that, if the tunnel barrier is replaced by a poor conductor with a large magnetization-dependent resistivity and a large spin diffusion constant, the spin and charge tunnel transport through the MTJ is adequately described by a drift-diffusion approach. The generalized spin-charge drift-diffusion model has been successfully applied to determine the spin accumulation and the torques acting on the magnetization in an MTJ structure. We compare the switching time distribution obtained under a fixed voltage, a fixed current, and a fixed current density through an MTJ. We demonstrate that all three approaches give similar switching time distributions, provided that the current values are properly adjusted.

2. MAGNETIZATION DYNAMICS IN STT-MRAM

The key element in modern magnetic memories is the MTJ. This structure is a sandwich of two ferromagnetic layers, usually composed of CoFeB, and an oxide layer, typically MgO, cf. Fig. 1. The binary information is stored as the relative orientation of the magnetization in the magnetic layers of the MTJ, as when the magnetization vectors are in a parallel state (P), the resistance is lower than in the anti-parallel state (AP). The difference in

Further author information: (Send correspondence to Simone Fiorentini)

Simone Fiorentini: E-mail: fiorentini@iue.tuwien.ac.at, Telephone: +43 1 58801 36017

Spintronics XIII, edited by Henri-Jean M. Drouhin, Jean-Eric Wegrowe,
Manijeh Razeghi, Proc. of SPIE Vol. 11470, 114701B · © 2020 SPIE
CCC code: 0277-786X/20/\$21 · doi: 10.1117/12.2567480

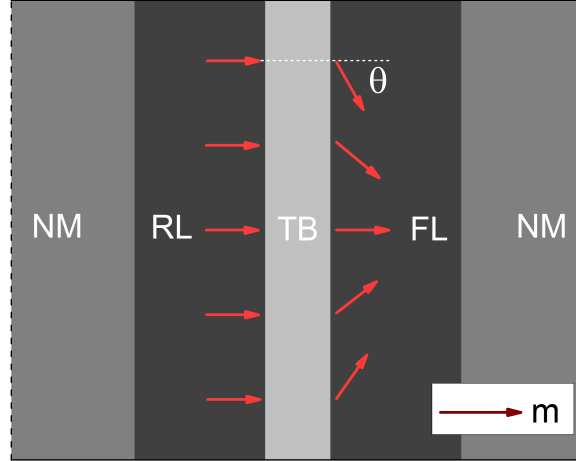


Figure 1: MTJ structure with non-uniform magnetization configuration. The structure is composed of a reference layer (RL), a tunnel barrier (TB), a free layer (FL), and two non-magnetic contacts (NM).

resistance can be read by an electric current passing through the structure. Thanks to the spin-transfer torque, switching between P and AP can be achieved by means of an electric current following the same path as the one used for reading. When the electrons cross the fixed reference layer (RL), they become spin-polarized, generating a spin current. They then enter the free layer (FL), where the spin current acts on the magnetization via the exchange interaction, generating the spin-transfer torque.⁸ If the current is sufficiently strong, the magnetization of the free layer can be switched between the two stable configurations, parallel or anti-parallel, relative to the reference layer. MTJs are characterized by their tunneling magnetoresistance ratio (TMR), defined as

$$TMR = \frac{G_P - G_{AP}}{G_{AP}}, \quad (1)$$

where G_P (G_{AP}) is the conductance in the P (AP) state. A high TMR is important to be able to read the conductance difference between the two configurations. In modern devices the TMR reaches values of 200% and higher.⁹

Thanks to interface-induced perpendicular anisotropy, thin layers of CoFeB on MgO are perpendicularly magnetized. The switching currents with this magnetization configuration are lower than the ones of in-plane magnetized structures, as in the former scenario current-driven and thermally-assisted switching go over the same energy barrier. The magnetization in the FL can be switched, while in the RL it is fixed, usually by antiferromagnetic exchange coupling to a pinned layer.¹⁰

Simulations of STT-MRAM switching involve the computation of magnetization dynamics. A solution of the Landau-Lifshitz-Gilbert (LLG) equation is required. When including the effect of spin transfer torque, this equation reads

$$\frac{\partial \mathbf{m}}{\partial t} = -\gamma \mu_0 \mathbf{m} \times \mathbf{H}_{\text{eff}} + \alpha \mathbf{m} \times \frac{\partial \mathbf{m}}{\partial t} + \frac{1}{M_S} \mathbf{T}_S, \quad (2)$$

where \mathbf{m} is the magnetization unit vector, γ is the gyromagnetic ratio, μ_0 is the magnetic permeability, α is the Gilbert damping constant, and M_S is the saturation magnetization. \mathbf{H}_{eff} is an effective field including various contributions, mainly the external field, the anisotropy field, the exchange interaction, the demagnetizing field, and thermal fluctuations. The term \mathbf{T}_S could be described by assuming a Slonczewski-like torque approach.¹¹ This, however, allows to approximately simulate the magnetization dynamics of the free layer only. A more complete description of the process can be obtained by computing the non-equilibrium spin accumulation \mathbf{S} across the whole structure. In this case, \mathbf{T}_S can be expressed as

$$\mathbf{T}_S = -\frac{D_e}{\lambda_J^2} \mathbf{m} \times \mathbf{S} - \frac{D_e}{\lambda_\varphi^2} \mathbf{m} \times (\mathbf{m} \times \mathbf{S}), \quad (3)$$

where λ_J is the exchange length, λ_φ is the spin dephasing length, and D_e is the electron diffusion coefficient. \mathbf{S} is generated when an electric current passes through the structure and gets polarized by the magnetic layers. In order to obtain \mathbf{S} , coupled spin and charge transport must be determined. When dealing with a spin valve, where the two ferromagnetic layers are separated by a conductive metal layer, it is sufficient to solve the spin and charge drift-diffusion equations in the structure.¹² However, in an MTJ the two ferromagnets are separated by a tunnel barrier. It is therefore necessary to find a way to incorporate the tunnel junction properties when solving the drift-diffusion equations.

3. MTJ MODEL AND RESULTS

In an MTJ, the amount of current flowing through the structure is mainly determined by the tunneling resistance, as it is much larger than the resistances of the ferromagnetic layers. As Ohm's law holds, the physical origin leading to the high resistivity is not important. Therefore, we model the tunnel barrier as a poor conductor whose low conductivity depends on the relative magnetization vectors' orientation as

$$\sigma(\theta) = \frac{\sigma_P + \sigma_{AP}}{2} \left(1 + \left(\frac{TMR}{2 + TMR} \right) \cos \theta \right), \quad (4)$$

where $\sigma_{P(AP)}$ is the conductivity in the P(AP) state, and θ is the local angle between the magnetic vectors in the free and reference layer. To obtain the current, we solve

$$\nabla \cdot (\sigma \nabla V) = 0, \quad (5a)$$

$$\mathbf{J}_C = \sigma \nabla V, \quad (5b)$$

where σ is the conductivity, V is the electrical potential and J_C is the charge current density. The equation is solved in the structure schematized in Fig.1. The potential is fixed with Dirichlet conditions on the left and right boundary, respectively. The conductivity is described by (4) in the tunneling layer, while it is constant in the ferromagnetic layers and the non-magnetic leads. The current density for this scenario was computed via the finite element method and is shown in Fig.2. The result is highly non-uniform and depends strongly on the position, with the difference between highest and lowest values of the perpendicular component of the current dictated by the TMR. The modulus of the in-plane current density is redistributed in order to accommodate

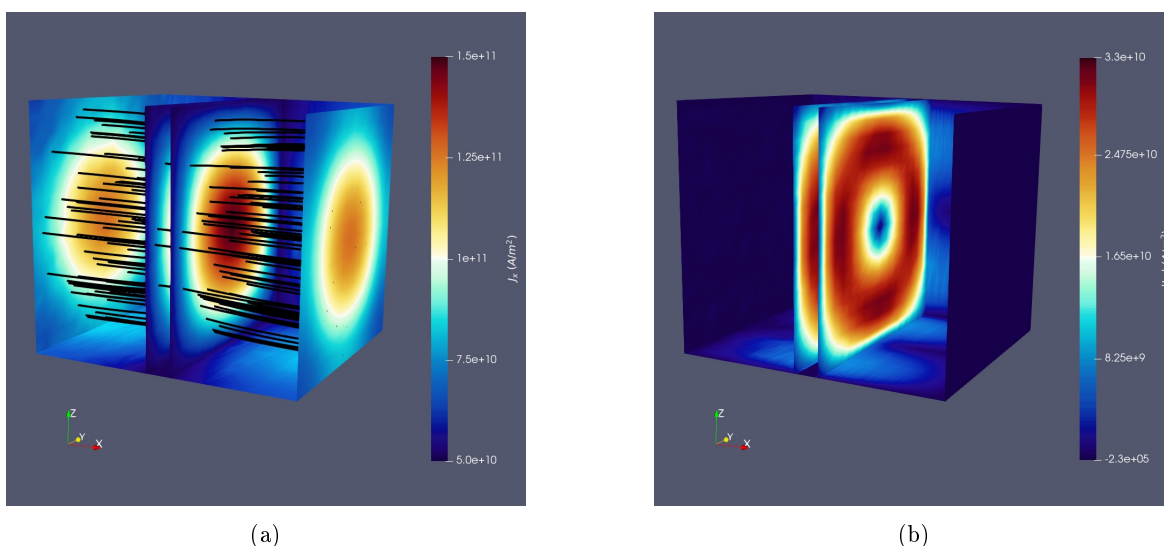


Figure 2: Current density distribution through a square MTJ with non-uniform FL magnetization. (a) The x-component (perpendicular) of the current density is larger for aligned magnetization vectors because of the lower resistance. (b) Due to the conservation of the current flow, it is redistributed in the yz-plane in the metal layers.

for the varying conductivity in the middle layer. Once \mathbf{J}_C is known, the spin current density \mathbf{J}_S and the spin accumulation \mathbf{S} through the barrier are found as¹³

$$\mathbf{J}_S = \frac{\mu_B}{e} \beta_\sigma \left(\mathbf{J}_C + \beta_D D_e \frac{e}{\mu_B} [(\nabla \mathbf{S}) \cdot \mathbf{m}] \right) \otimes \mathbf{m} - D_e \nabla \mathbf{S}, \quad (6a)$$

$$-\nabla \mathbf{J}_S - D_e \left(\frac{\mathbf{S}}{\lambda_{sf}^2} + \frac{\mathbf{S} \times \mathbf{m}}{\lambda_J^2} + \frac{\mathbf{m} \times (\mathbf{S} \times \mathbf{m})}{\lambda_\varphi^2} \right) = 0, \quad (6b)$$

where μ_B is the Bohr magneton, e is the electron charge, β_σ and β_D are polarization parameters, and λ_{sf} is the spin-flip length. In order to adequately model the properties of a tunnel barrier, it is not sufficient to deal only with the electrical characteristics of the structure. The spin accumulation must be preserved across the barrier without spin flips. The equation for \mathbf{S} in the middle layer reduces to

$$D_S \nabla^2 \mathbf{S} - D_S \frac{\mathbf{S}}{\lambda_{sf}^2} = 0, \quad (7)$$

where D_S is the spin diffusion constant inside the barrier. To achieve spin continuity across the tunneling layer, one must neglect the spin relaxation by setting all scattering lengths to infinity. However, this is not sufficient. The spin diffusion coefficient in the middle region must also be set large compared to the electron diffusion coefficient in the ferromagnetic layers, as reported in Fig.3(a). When the two coefficients have the same value, the spin accumulation decays through the tunnel barrier, while the choice of a large spin diffusion coefficient reduces the slope in the middle layer to the point that the spin accumulation is practically preserved. The solution in the whole structure is reported in Fig.3(b). The non-magnetic leads are necessary, in a multilayer structure, to ensure decay of the spin accumulation through proper boundary conditions. With \mathbf{S} known, we compute the torques acting on both ferromagnetic layers, which are reported in Fig.4(a). The dependence of the torque on the spin diffusion coefficient is reported in Fig.4(b), which shows that, provided a large enough value of the coefficient, the torque is independent of it. This torque is then inserted in the LLG equation to resolve the magnetization dynamics.

For the computation of torques with the proposed scheme, we employed the assumption of a fixed voltage at switching, which is a typical situation in many practical applications. In contrast, the usual approach for

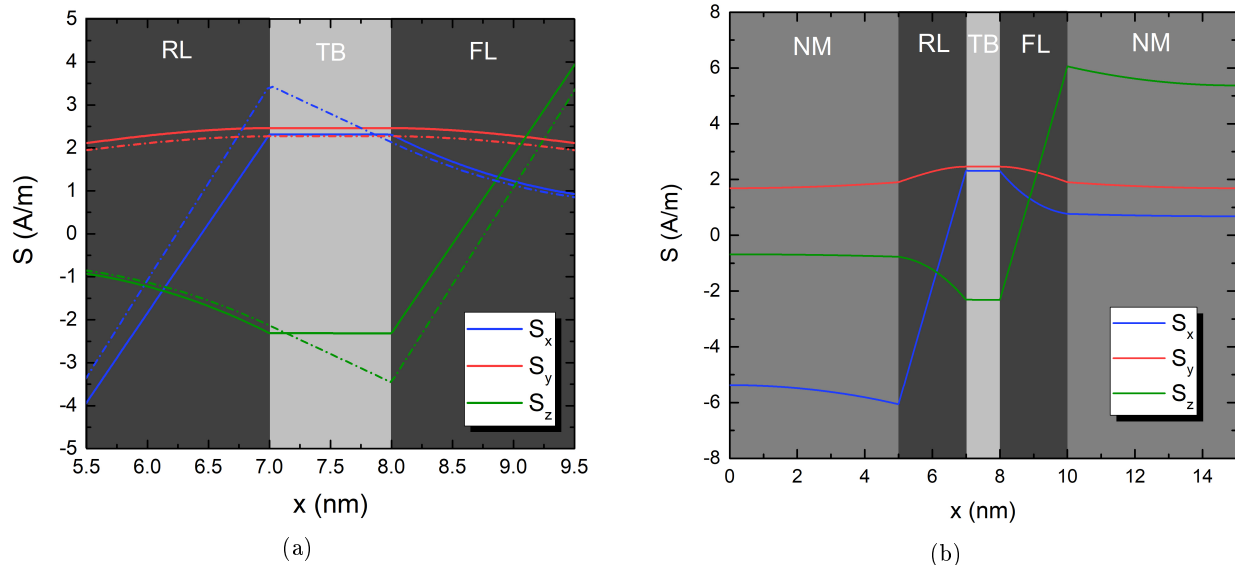


Figure 3: Spin accumulation across the tunneling layer. The magnetization lies along x in the FL and along z in the RL. (a) Close-in on the tunnel layer. The dashed lines are computed using the same value for D_S in the TB and D_e in the FL and the RL, while solid lines use a very high value of D_S , which renders \mathbf{S} constant across the TB. (b) Spin accumulation solution across the whole structure.

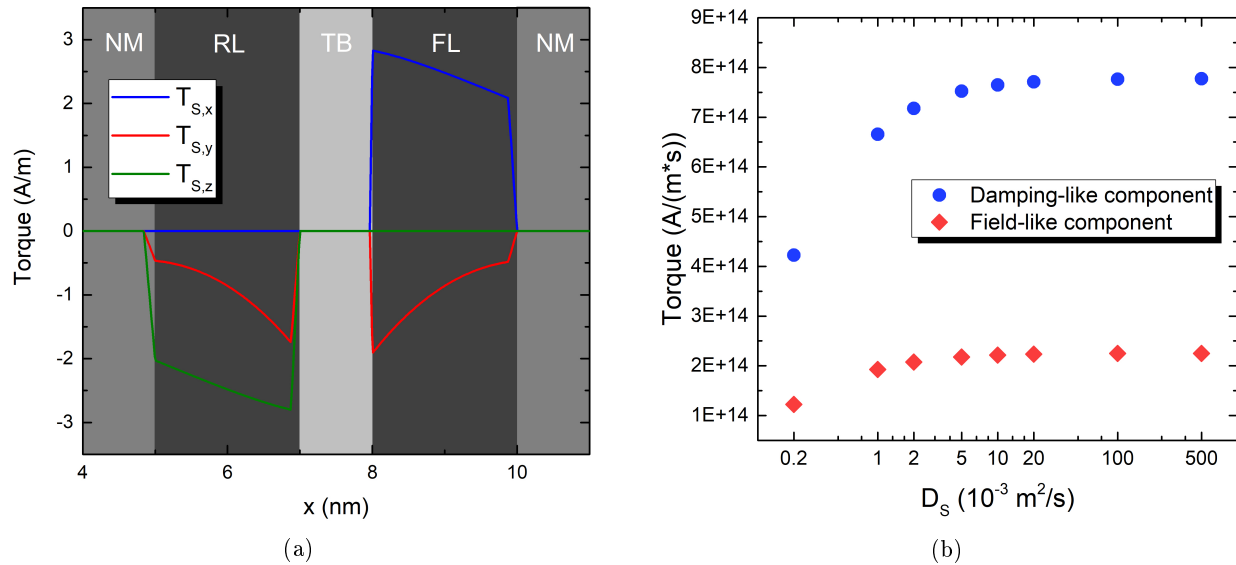


Figure 4: Torque computed from the spin accumulation. (a) The spin drift-diffusion approach permits to compute the torques acting on both layers, FL and RL. (b) Magnitude of the torque in the FL as a function of the spin diffusion coefficient in the TB. At high values of the coefficient, torques do not depend on it.

micromagnetic simulations of STT switching is to assume a constant and uniform current density. As shown previously, the current density becomes highly non-uniform during the switching process, so this assumption is violated. In order to evaluate the validity and the limits of the fixed current density approach in computing the switching time, we compare it with the fixed voltage approach and with a model in which the total current is fixed and redistributed according to the local magnetization orientation, and thus to the local resistance.¹⁴ We define the total current at which the switching is performed to be equal to the voltage divided by the resistance in the initial parallel (P) or anti-parallel (AP) state. The switching times at room temperature depend on the realization of the stochastic field which mimics the magnetization fluctuations. By using a fixed layer antiferromagnetically

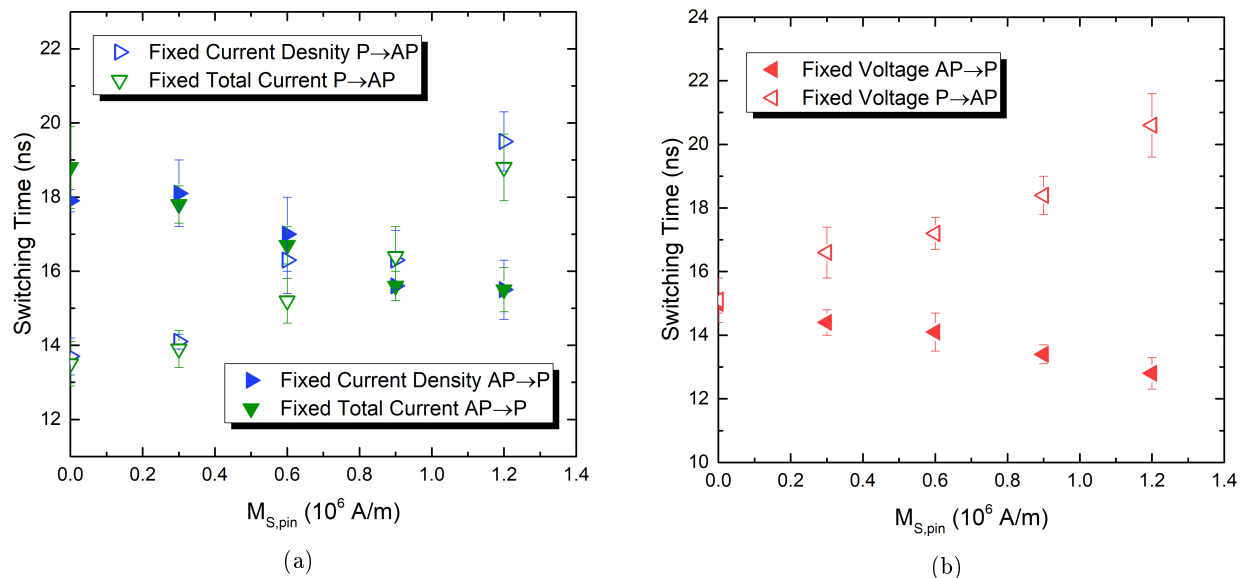


Figure 5: Comparison between AP→P and P→AP switching for various levels of the uncompensated stray field at $T=300 \text{ K}$. The bars show switching time variations due to thermal fluctuations. (a) Distribution for the fixed current density and fixed total current approaches. (b) Distribution for the fixed voltage approach.

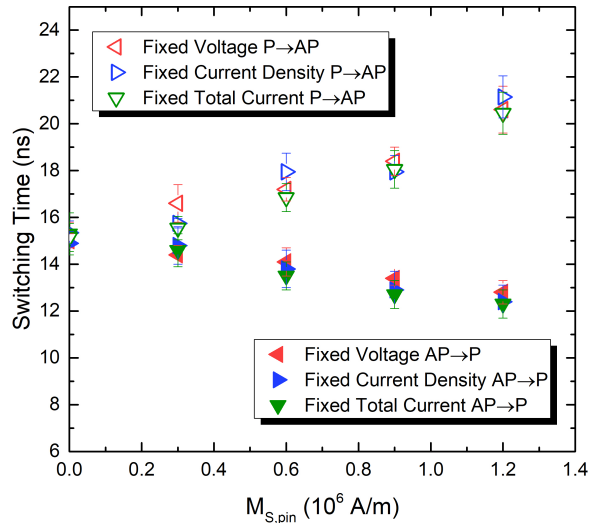


Figure 6: Comparison of switching times for the tuned values of input currents at $T=300$ K. The switching times of all three models are compatible within the thermal variation.

coupled to the reference layer, one can compensate the total stray field acting on the free layer. We computed the switching time distribution for the three approaches under different values of the uncompensated stray field coming from the reference layer. The stray field is modeled by the total saturation magnetization of the antiferromagnetically coupled layers. The results are reported in Fig.5. Compensating the stray field results in a higher switching time for the AP→P configuration and a lower one for P→AP. However, the results for switching times are 15% higher for AP→P and 10% lower for P→AP for the fixed current approaches as compared to the fixed voltage one. The difference is due to the fact that in the fixed voltage approach, the total current is allowed to adapt to the varying resistance. In order to compensate this effect, we adjust the currents in the other two approaches to make them 9% higher for AP→P and 4% lower for P→AP switching. The resulting switching times are shown in Fig.6. With this tuned choice of currents, all the models produce compatible results within the thermal spread, so the simplified description offered by the fixed current density approach is still a good approximation for high TMR perpendicular structures, provided the currents are appropriately chosen.

4. CONCLUSION

We proposed a method for applying the spin and charge drift-diffusion formalism in computing the torques acting on the magnetization in an MTJ structure. The current density can be properly described by modeling the tunnel layer as a poor conductor whose conductivity is locally dependent on the relative magnetization vectors' orientation in the free and reference layer, with fixed voltage at the contacts. In order to preserve the spin accumulation through the tunnel barrier, we showed that it is necessary to put all scattering lengths to infinity and assume a high diffusion coefficient in the middle layer. This generalized spin and charge drift-diffusion approach can be successfully applied to determine the torques acting on the magnetization in a modern STT-MRAM device, in order to compute the magnetization dynamics. We also compared the switching time distribution in the realistic fixed voltage scenario to two approximate fixed current approaches and showed that, provided that the current values are properly adjusted, all three models give comparable results. This allows the use of the approximate fixed current density approach to accurately compute the switching time of an STT-MRAM device in a fast way.

ACKNOWLEDGMENTS

The financial support by the Austrian Federal Ministry for Digital and Economic Affairs and the National Foundation for Research, Technology and Development is gratefully acknowledged.

REFERENCES

- [1] Sakhare, S., Perumkunnil, M., Bao, T. H., Rao, S., Kim, W., Crotti, D., Yasin, F., Couet, S., Swerts, J., Kundu, S., Yakimets, D., Baert, R., Oh, H., Spessot, A., Mocuta, A., Kar, G. S., and Furnemont, A., "Enablement of STT-MRAM as last level cache for the high performance computing domain at the 5nm node," *Proc. of the 2018 IEDM*, 18.3.1–18.3.4 (2018).
- [2] Aggarwal, S., Almasi, H., DeHerrera, M., Hughes, B., Ikegawa, S., Janesky, J., Lee, H. K., Lu, H., Mancoff, F. B., Nagel, K., Shimon, G., Sun, J. J., Andre, T., and Alam, S. M., "Demonstration of a reliable 1 Gb standalone spin-transfer torque MRAM for industrial applications," *Proc. of the 2019 IEDM*, 2.1.1–2.1.4 (2019).
- [3] Alzate, J. G., Arslan, U., Bai, P., Brockman, J., Chen, Y. J., Das, N., Fischer, K., Ghani, T., Heil, P., Hentges, P., Jahan, R., Littlejohn, A., Mainuddin, M., Ouellette, D., Pellegren, J., Pramanik, T., Puls, C., Quintero, P., Rahman, T., Sekhar, M., Sell, B., Seth, M., Smith, A. J., Smith, A. K., Wei, L., Wiegand, C., Golonzka, O., and Hamzaoglu, F., "2 Mb array-level demonstration of STT-MRAM process and performance towards L4 cache applications," *Proc. of the 2019 IEDM*, 2.4.1–2.4.4 (2019).
- [4] Gallagher, W. J., Chien, E., Chiang, T., Huang, J., Shih, M., Wang, C. Y., Weng, C., Chen, S., Bair, C., Lee, G., Shih, Y., Lee, C., Lee, P., Wang, R., Shen, K. H., Wu, J. J., Wang, W., and Chuang, H., "22nm STT-MRAM for reflow and automotive uses with high yield, reliability, and magnetic immunity and with performance and shielding options," *Proc. of the 2019 IEDM*, 2.7.1–2.7.4 (2019).
- [5] Hu, G., Nowak, J. J., Gottwald, M. G., Brown, S. L., Doris, B., D'Emic, C. P., Hashemi, P., Houssameddine, D., He, Q., Kim, D., Kim, J., Kothandaraman, C., Lauer, G., Lee, H. K., Marchack, N., Reuter, M., Robertazzi, R. P., Sun, J. Z., Suwannasiri, T., Trouilloud, P. L., Woo, S., and Worledge, D. C., "Spin-transfer torque MRAM with reliable 2 ns writing for last level cache applications," *Proc. of the 2019 IEDM*, 2.6.1–2.6.4 (2019).
- [6] Lee, K., Bak, J. H., Kim, Y. J., Kim, C. K., Antonyan, A., Chang, D. H., Hwang, S. H., Lee, G. W., Ji, N. Y., Kim, W. J., Lee, J. H., Bae, B. J., Park, J. H., Kim, I. H., Seo, B. Y., Han, S. H., Ji, Y., Jung, H. T., Park, S. O., Kwon, O. I., Kye, J. W., Kim, Y. D., Pae, S. W., Song, Y. J., Jeong, G. T., Hwang, K. H., Koh, G. H., Kang, H. K., and Jung, E. S., "1Gbit high density embedded STT-MRAM in 28nm FDSOI technology," *Proc. of the 2019 IEDM*, 2.2.1–2.2.4 (2019).
- [7] Naik, V. B., Lee, K., Yamane, K., Chao, R., Kwon, J., Thiyagarajah, N., Chung, N. L., Jang, S. H., Behin-Aein, B., Lim, J. H., Lee, T. Y., Neo, W. P., Dixit, H., K, S., Goh, L. C., Ling, T., Hwang, J., Zeng, D., Ting, J. W., Toh, E. H., Zhang, L., Low, R., Balasankaran, N., Zhang, L. Y., Gan, K. W., Hau, L. Y., Mueller, J., Pfefferling, B., Kallensee, O., Tan, S. L., Seet, C. S., You, Y. S., Woo, S. T., Quek, E., Siah, S. Y., and Pellerin, J., "Manufacturable 22nm FD-SOI embedded MRAM technology for industrial-grade MCU and IoT applications," *Proc. of the 2019 IEDM*, 2.3.1–2.3.4 (2019).
- [8] Slonczewski, J., "Current-driven excitation of magnetic multilayers," *Journal of Magnetism and Magnetic Materials* **159**(1), L1 – L7 (1996).
- [9] Skowroński, W., Czapkiewicz, M., Ziętek, S., Chęciński, J., Frankowski, M., Rzeszut, P., and Wrona, J., "Understanding stability diagram of perpendicular magnetic tunnel junctions," *Scientific Reports* **7**(1), 10172 (2017).
- [10] Bhatti, S., Sbiaa, R., Hirohata, A., Ohno, H., Fukami, S., and Piramanayagam, S., "Spintronics based random access memory: A review," *Materials Today* **20**(9), 530 – 548 (2017).
- [11] Slonczewski, J. C., "Currents, torques, and polarization factors in magnetic tunnel junctions," *Physical Review B* **71**, 024411 (2005).
- [12] Abert, C., Ruggeri, M., Bruckner, F., Vogler, C., Hrkac, G., Praetorius, D., and Suess, D., "A three-dimensional spin-diffusion model for micromagnetics," *Scientific Reports* **5**(1), 14855 (2015).
- [13] Lepadatu, S., "Unified treatment of spin torques using a coupled magnetisation dynamics and three-dimensional spin current solver," *Scientific Reports* **7**(1), 12937 (2017).
- [14] Aurélio, D., Torres, L., and Finocchio, G., "Magnetization switching driven by spin-transfer-torque in high-TMR magnetic tunnel junctions," *Journal of Magnetism and Magnetic Materials* **321**(23), 3913 – 3920 (2009).